

Northern Illinois University

Design And Construction Of A Hexapod Walking Robot

A Thesis Submitted to the
University Honors Program
In Partial Fulfillment of the
Requirements of the Baccalaureate Degree
With Upper Divisional Honors
Department of Mechanical Engineering

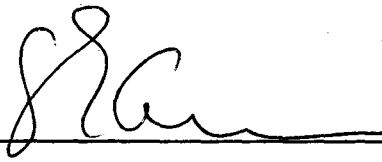
by

Paul David Wanthal

DeKalb, Illinois

August, 1996

Student name: WANTHAL, PAUL

Approved by:  5/6/96

Department of: MECHANICAL ENGINEERING

Date: 5/6/96

**HONORS THESIS ABSTRACT
THESIS SUBMISSION FORM**

AUTHOR: Paul D. Wanthal

THESIS TITLE: Design And Construction Of A Hexapod Walking Robot

ADVISOR: Sengoda Ganesan, Ph.D., P.E. **ADVISOR'S DEPARTMENT:** Mechanical Engineering

DISCIPLINE: Mechanical Engineering

PAGE LENGTH: 28

BIBLIOGRAPHY: Yes

ILLUSTRATED: Yes

PUBLISHED: No

LIST PUBLICATION: --

COPIES AVAILABLE (HARD COPY, MICROFILM, DISKETTE): Yes, hard copy available in the library in the Engineering Building.

ABSTRACT:

The design and construction of a hexapod walking robot for the purpose of continuing research in robot architecture and behavior will be discussed. A short description of common robot designs is given, followed by a discussion of the basic design that was selected. Linear actuator design, frame design, and leg design is detailed. A description of the analog servo control system and the functional requirements of the microcontroller system is included. The lithium batteries chosen for the power supply are discussed. A schedule for project completion is given, as well as component costs. Performance of the robot was limited somewhat by RF interference which caused problems in the digital circuitry as well as the analog circuitry used. A brief discussion of possible solutions to this problem is given.

ABSTRACT

The design and construction of a hexapod walking robot for the purpose of continuing research in robot architecture and behavior will be discussed. A short description of common robot designs is given, followed by a discussion of the basic design that was selected. Linear actuator design, frame design, and leg design is detailed. A description of the analog servo control system and the functional requirements of the microcontroller system is included. The lithium batteries chosen for the power supply are discussed. A schedule for project completion is given, as well as component costs. Performance of the robot was limited by RF interference which caused problems in the digital circuitry as well as the analog circuitry used. A brief discussion of possible solutions to this problem is given.

A related project, *Microprocessor Design For A Walking Robot*, by Christopher Johnson, Northern Illinois University Department Of Electrical Engineering, May 1996, contains a detailed description of the microcontroller system and programming for this robot.

TABLE OF CONTENTS

List of Figures.....	i
List of Tables.....	i
List of Appendices.....	i
List of Variables.....	ii
Introduction.....	1
Selection of Basic Design	1
Actuator Design	2
Frame Design.....	3
Leg Design	4
Servo Control Circuitry	6
Power Supply.....	8
Control Interface System	9
Microcontroller.....	11
Walking Algorithm	12
Design Program	13
Discussion of Results.....	13
Conclusion.....	14
Bibliography	15
Acknowledgments.....	15
Appendices.....	16

LIST OF FIGURES

1. Linear Actuator Design	3
2. Frame Layouts	4
3. Pivot Block Detail.....	4
4. Frame/Truss Configuration.....	4
5. Leg Configuration	5
6. Top View Of Robot.....	6
7. Servo Control Circuit.....	7
8. Interface Circuit.....	9
9. Process Feedback.....	11
10. Leg Configurations During Motion.....	12

LIST OF TABLES

1. Program Development.....	13
-----------------------------	----

LIST OF APPENDICES

1. Appendix A, Actuator Analysis.....	16
2. Appendix B, Joint Relationships	20
3. Appendix C, Battery Specifications.....	23
4. Appendix D, Motor Specifications	24
5. Appendix E, Microcontroller Board	26
6. Appendix F, Printed Circuit Board Layouts	27

LIST OF VARIABLES

For continuity, the variables and functions listed are grouped together with respect to their appearance in the main report and appendices.

Main Report Variables:

r_1	Resistance 1.
r_2	Resistance 2.
$V_{\text{differential}}$	The total voltage drop across both resistors in the voltage divider.
V_{junction}	The voltage drop at the junction of the voltage divider, measured with respect to ground.
V_{supply}	The supply voltage for the voltage divider.

Appendix A variables

A_b	Radial bearing area of gear shaft on gearbox.
A_{shaft}	Circumferential area of shaft in contact with an idler gear.
d	Radial interference.
d_1	Pitch diameter of pinion gear and small idler gear.
d_2	Pitch diameter of lead screw drive gear and large idler gear.
d_m	Mean lead screw diameter.
d_n	Nominal lead screw diameter.
E	Young's modulus.
F_f	Frictional force on idler shaft.
F_{idler}	Idler shaft reaction force.
F_l	Lead screw shaft reaction force.
F_n	Normal force on idler shaft.
F_r	Radial force.
F_t	Tangential force.
F_{12r}	Radial force component of pinion on idler.
F_{12t}	Tangential force component of pinion on idler.
F_{23x}	Force on idler shaft in x direction.
F_{23y}	Force on idler shaft in y direction.
F_{43r}	Radial force component of lead screw drive gear on idler.
F_{43t}	Tangential force component of lead screw drive gear on idler.
ID	Inner diameter of thrust collar bearing.
l	Lead screw pitch.
l_{max}	Maximum calculated actuator load.
OD	Outer diameter of thrust collar bearing.
P	Power.
P_s	Minimum pressure required for no slippage.
P_t	Pressure at shrink fit transition.

Appendix A variables, continued

R	Idler shaft radius.
r_i	Inner shaft radius.
r_o	Outer shaft radius.
V_{\max}	Maximum motor speed.
V_{out}	Lead screw rotational speed.
β_1	Coefficient of friction for like metals.
β_2	Coefficient of friction in gearbox.
ϕ	Pressure angle.
μ_s	Coefficient of friction for lead screw.
σ_{bi}	Idler bearing stress.
σ_{bl}	Lead screw bearing stress.
σ_{bc}	Thrust collar bearing stress.
τ_{avail}	Available torque at lead screw.
τ_{idler}	Torque on idler shaft.
τ_{ls}	Torque at lead screw.
τ_{\max}	Maximum motor torque.

Appendix B variables

A_{an}	The angle between R_{an} and horizontal.
a_n	Hip rotation joint axis angle.
C_e	Horizontal distance from hip axis to foot.
F	Approximate load on foot.
F_{han}	Force in hip elevation actuator.
F_{kan}	Force in knee actuator.
G	Ground clearance.
H_{elev}	Hip elevation angle measured from horizontal.
$H_{\text{elev}}^{\text{diff}}$	Total change in hip elevation angle.
K_{bend}	Knee joint angle.
$K_{\text{bend}}^{\text{diff}}$	Total change in knee joint angle.
l_1	Upper leg length.
l_2	Lower leg length.
l_{1k}	Knee actuator mounting point on upper leg measured from knee.
l_{2k}	Knee actuator mounting point on lower leg measured from knee.
R_{an}	Slant distance from hip to foot.
S	Distance from hip elevation joint to hip elevation actuator mounting point along hip rotation axis.
Stride	Stride length.
α	Starting angle for hip rotation axis.
λ	Angle between l_1 and l_{1k} .

INTRODUCTION

The development and use of robots in industry and research is becoming widespread, and the field of mobile robotics is no exception. While the use of mobile robots in everyday applications is still limited by high research and development costs, they have become invaluable in applications where risk of injury is high, such as the nuclear industry and planetary exploration.

There are many different types of mobile robots, the designs of which vary greatly with application. Mobile robots may be distinguished by many characteristics: their levels of perception, methods of control, or type of locomotion, to name a few of the most important features. The last feature, locomotion, is the subject of this study.

The locomotion methods employed by designers are as diverse as the applications to which the robots are put. Wheeled platforms are often the system of choice because of their simplicity and reliability. However, with the advent of small scale microcontrollers and improved servo control technology, more complicated locomotion systems are becoming possible. Among the most interesting of these designs are the legged walking platforms, whether they be of the "frame walker" type, which consist of a pair of frames which are capable of motion relative to one another and to which the legs are attached, or platforms which are equipped with legs capable of independent motion. It is this latter case which is discussed. This design, while more complex than wheeled platforms or frame walkers, possesses greater mobility and is more robust mechanically due to the redundancy of independent drive mechanisms (legs).

Because most of these units are designed for limited applications, mainly research in artificial intelligence and control architecture, their cost is typically high, often placing them out of reach of individual purchasers. It is for this reason, as well as the experience gained by the design and construction of such a device, that the legged walking platform was selected for construction.

SELECTION OF BASIC DESIGN

There are several aspects of chassis design that are open to selection once the decision has been made to construct a walking robot. Among these are the number of legs, the general shape of the body (frame), the number of degrees of freedom per leg, layout of components, and overall dimensions of the unit.

Some considerations when choosing the number of legs are stability, complexity, and the desired gait pattern of the robot. A walking robot possessing four legs is stable and is the least complex physically, but a difficulty arises in the control architecture because such a design requires a dynamic gait, that is, one which requires the vehicle's weight to shift from one leg or legs to another during motion. Such gait patterns are much more difficult to implement than statically stable gaits.

Robots possessing six legs have good inherent stability and a variety of statically stable gait patterns to choose from. The only drawback to this configuration is increased mechanical complexity as compared to the four legged design .

When a robot possessing eight or more legs is designed, the problems of mechanical complexity, gait selection, and joint coordination increase with each additional pair of legs (assuming legs are added in pairs). Stability is excellent, but does not increase as dramatically from six legs to eight as from four to six.

From this brief analysis of the positive and negative aspects of each of the above configurations, a hexapod is the logical choice for a walking platform.

Body shape is the next aspect of design that must be addressed. This design feature is perhaps not as influential in the function of the robot as the others discussed in this section, therefore there is more latitude for a design which is aesthetically pleasing, yet functional. Weight and ease of design for motion are two aspects of body design which are examined.

Rather than solid body panels to which components are attached, an open truss frame design is chosen to which components can be mounted both internally and externally. This gives strength to the design while being lightweight; access to the interior of the unit is also facilitated without disassembly.

It is relatively simple to design the body for linear motion and almost any shape, whether elongated or round, will suffice. However, for ease of manufacture, a round or radially symmetric design simplifies the design due to the redundancy of parts; thus a design with radial symmetry was selected over an elongated design.

THE ACTUATORS

Before discussing the final design of the frame, it is necessary to examine the design of the actuators used for achieving leg motion, as their design will influence the frame dimensions and, to some extent, the frame layout. Rather than choosing actuators "off the shelf", servos capable of generating large forces were constructed specifically for the robot at low material cost (the time expenditure, while substantial, was justified by the experience gained during the manufacturing processes involved). Because of tooling limitations [1], rotary servos were eliminated because of the high number of gears required for large force multiplication. Linear actuators proved to be a better alternative because the combination of gearing and a lead screw provided high mechanical advantage with few gears. For ease of manufacture, all actuators in the robot were of the same design. The actuators used in the robot consist of a gearbox through which the torque of the attached drive motor is increased and delivered to a lead screw. A ram travels along the lead screw, producing linear motion from rotary. Actuator specifications are as follows:

Drive motor:	Globe 3A683 (Appendix D)
Nominal voltage range:	24 - 29 VDC
Speed:	16000 RPM at rated load
Torque:	1 in oz (7.06E-3 N m) nominal rated load
Maximum current:	1.0 amp at rated load

[1] Gear production was constrained by tooling limitations to gears with tooth numbers ranging from 12-13 teeth and 35-54 teeth, respectively (#8 and #3 cutters) with a 48 diametral pitch. Large gear reduction with few gears was not possible because of actuator size constraints.

Gear train:	4 spur gears, 16:1 reduction
Material:	AISI 1080
Pinion:	12 teeth, 48 diametral pitch, 14.5° pressure angle
Idler:	2 gears, common shaft; 48 teeth, 48 diametral pitch, 14.5° pressure angle
Lead screw drive gear:	12 teeth, 48 diametral pitch, 14.5° pressure angle 48 teeth, 48 diametral pitch, 14.5° pressure angle
angle	
Lead screw:	0.164 in (4.17 mm) dia, 8-32 NC pitch, 3 in (76.2 mm) travel
Material:	W-1
Ram:	0.375 in (9.53 mm) dia
Material:	W-1
Gearbox and ram guide material:	Aluminum, T6 temper

Figure 1 depicts a cutaway view of the actuator with major components indicated.

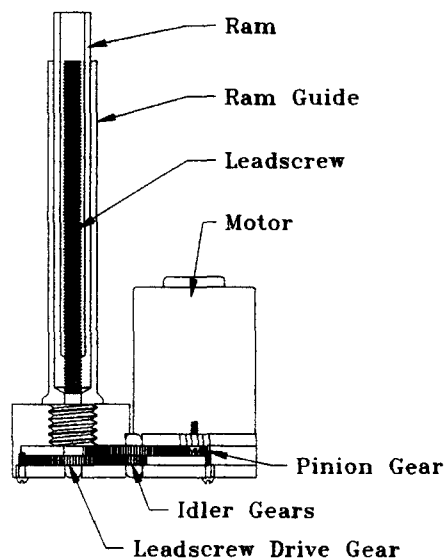


Figure 1. Linear Actuator Design

The original design of the actuators was analyzed for force output (Appendix A) and subsequently modified by the addition of thrust bearing surfaces and the use of improved lubricants, resulting in an increase of performance of approximately 100%.

THE FRAME

To simplify the construction of the frame and implement the radial symmetry described earlier, the frame was constructed of linear angle elements forming a pair of upper and lower hexagonal rings which are rigidly separated by a truss network. Leg attachment points are located at the six corners of the lower ring. The legs pivot on pins which pass through hip pivot blocks at the corners of the upper and lower rings.

Hip rotation actuators are mounted within the frame with the rams extending through the plane formed by the "flats" of the frame.

Figure 2a depicts an early design of the frame and actuator layout. This design was dropped in favor of the design shown in Figure 2b because of increased compactness of the latter design. The area within the frame in 2b inscribed by the circle is the payload area (interface, batteries, etc.). Other circuit boards were spaced around the periphery of the hexagonal rings, just inside the frame.

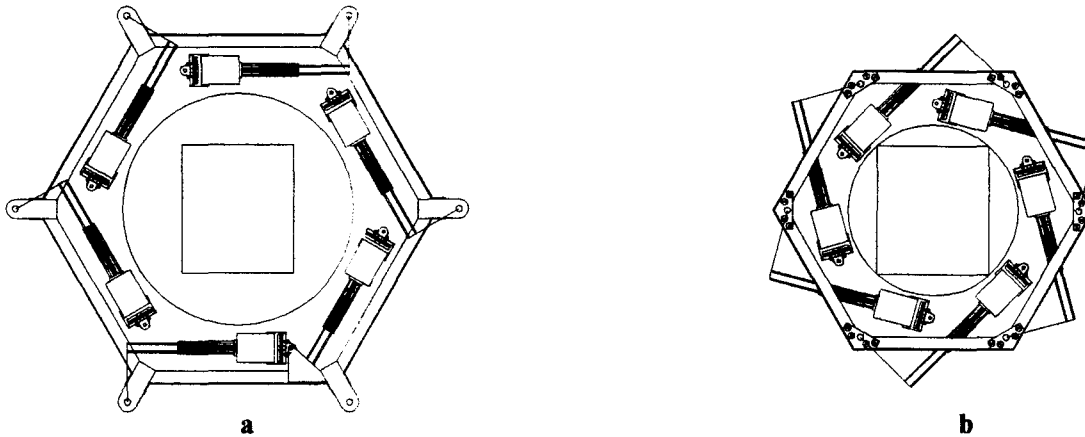


Figure 2. Frame Layouts

Frame ring elements were constructed of 19 gauge aluminum sheet formed into equal leg angle with a nominal leg dimension of 0.5 in (12.7 mm). The distance across the corners of the ring in Figure 2b is 12.55 in (318.8 mm). Truss elements were also made from 19 gauge aluminum sheet, formed into equal leg angle with a nominal leg dimension of 0.313 in (7.94 mm). Hip pivot blocks were machined from aluminum and assembled to the ring elements using 6-32 NC screws (Fig. 3). Truss elements were attached to the rings using 4-40 NC screws. A side view of the ring and truss assembly is shown in Figure 4.

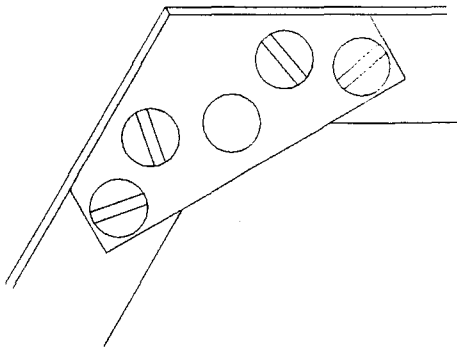


Figure 3. Pivot Block Detail

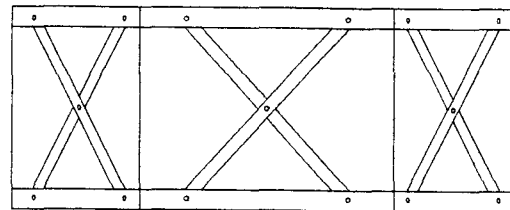


Figure 4. Frame/Truss Configuration

THE LEGS

Leg configuration was one of the most important considerations during design of the robot chassis.

A minimum of two degrees of freedom is required for motion: a hip rotation for propulsion and a hip or knee lift for returning the leg to the starting position for the next propulsion stroke. While functional, a two degree of freedom has, by definition, limited range of motion which often results in an up and down motion of the body as well as "skidding" of the foot relative to the ground. A three degree of freedom leg eliminates these problems by allowing true linear foot motion with the added benefit of precise foot placement anywhere within the reach of the leg. For this reason, a three degree of freedom leg was implemented for this system.

Although the limited control systems used did not allow full exploitation of the full range of motion characteristics possible, such as real time variable ride height, unlimited gait selection, and real time variable stance, they allowed an approximation of linear foot motion. However, these options were left open to future development with this type of design.

When designing the legs, the general range of motion had to be specified. For simplicity, the motion was limited to linear strides with the following input parameters: angular rotation of the hip, the lengths of the upper and lower legs, horizontal stance, and ground clearance. Output is the hip elevation angle and the knee bend angle required to produce the desired linear motion and the resulting stride length. The leg joint position and force relationships were developed and modeled using mathematical software (Appendix B).

The final leg design is depicted in Figure 5. The physical layout of the actuators for raising the hip joint and extending the knee was based on the angular parameters found in the kinematic analysis and was to some extent a trial and error process, with mathematical models being used to determine the force in each actuator throughout the entire range of motion (Appendix B). This was compared to the force the actuator was capable of exerting based on the actuator analysis and the leg design was adjusted accordingly by iteration until an acceptable solution was achieved. Although the range of motion is constrained to simple straight line walking and turning on a level surface, the joints were designed to have a range of motion allowing climbing and obstacle avoidance, in keeping with design for future improvements in control. The upper and lower leg sections were made of the same angle sections as the hexagonal rings of the frame (section 3, *The Frame*) and the hinges were machined from aluminum. Knee and hip elevation hinge pins were made from 0.313 in (7.94 mm) aluminum rod and the hip pivot pin was made of 0.25 in (6.35 mm) aluminum rod. Each leg was equipped with a hemispherical foot made of Delrin to allow slippage (skidding) if necessary, thereby reducing the load on the actuators.

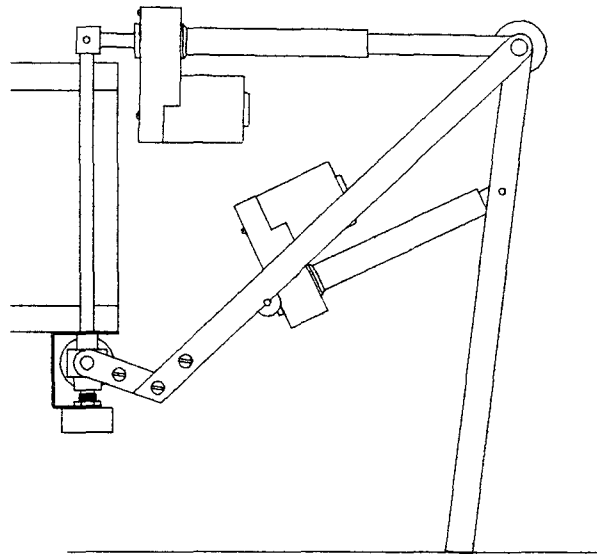


Figure 5. Leg Configuration

Figure 6 depicts the top view of the robot with the legs attached.

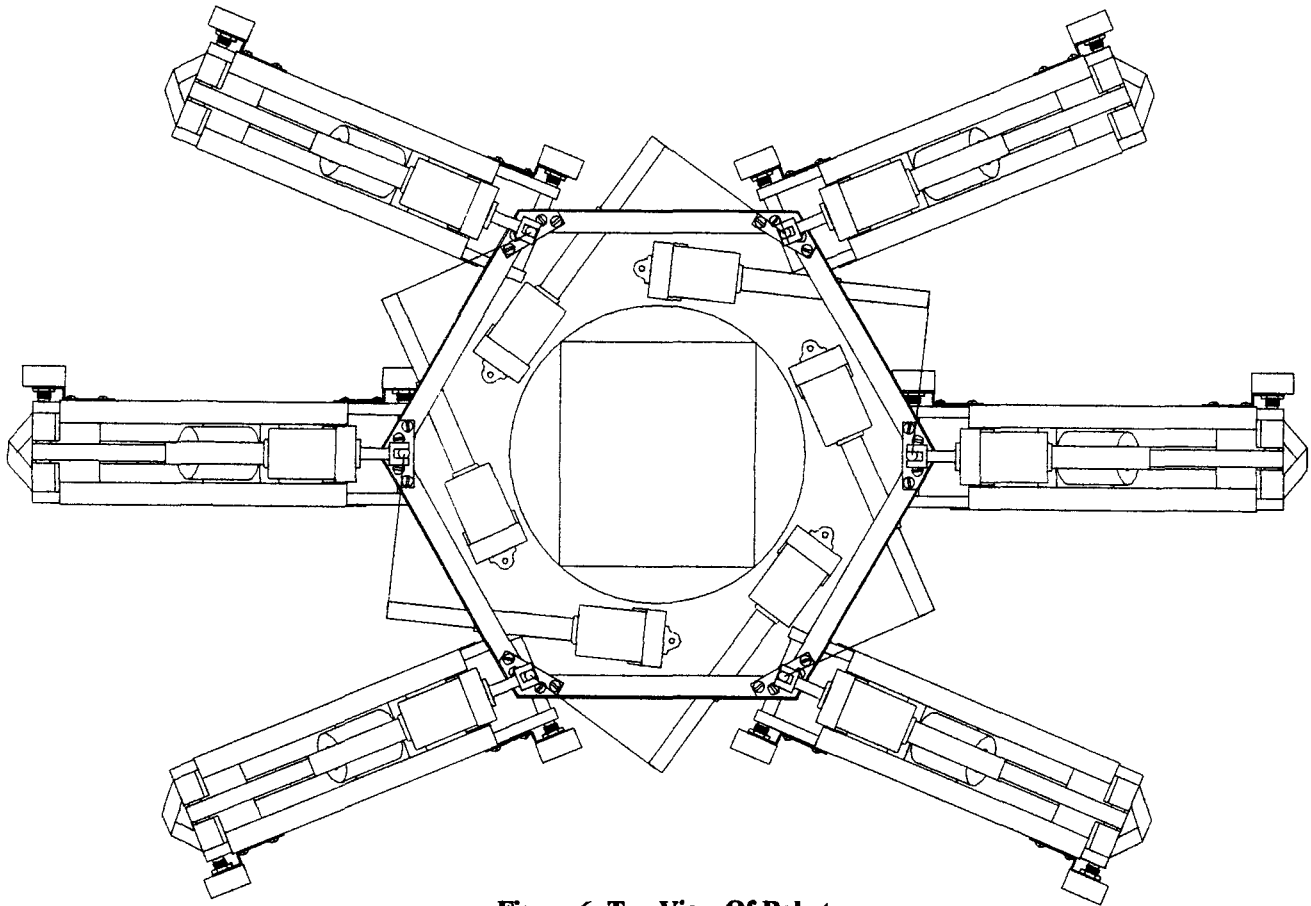


Figure 6. Top View Of Robot

SERVO CONTROL CIRCUITRY

The actuators in the legs are controlled by six servo controller circuit boards, one mounted on each leg (Figure 7). Each board consists of three 33030 servo controller chips, an LM324 operational amplifier and supporting circuitry. The position of each of the three joints in each leg is monitored using rotary potentiometers mounted coaxially with the hinge pins of each joint. The servo controller board possesses a three branch wheatstone bridge circuit; each potentiometer in the leg serves as a resistance in each branch. The branch containing the potentiometer which monitors hip rotation is used as the reference voltage to which the other two joints adjust themselves. Thus the actuators are directly controlled through servo controller chips, one chip to drive each actuator; the chip detects voltage differences across the bridge with respect to the reference branch and operates the actuator in the appropriate direction to minimize the difference. By choosing appropriate potentiometer values, the required angular relationship between the joints can be maintained closely, thus producing approximately linear motion at the foot. Mathematical models were used to help determine the position sensing potentiometer values given the required angle of rotation.

The leg lift required at the end of each propulsion stroke preparatory to return was accomplished through switching an extra resistance into the hip elevation branch of the wheatstone bridge circuit, upsetting the voltage balance in the bridge and prompting the servo controller to adjust the hip elevation to remove the perceived positional anomaly. The resulting change in hip elevation can be controlled through selecting the resistance that is switched into the bridge. Hip rotation direction control is accomplished by connecting the reference lines of the hip rotation servo controller chip across a two-branch wheatstone bridge.

With the bridge balanced, the servo controller chip is idle, however, a switching transistor is installed across each of the lower bridge resistances; applying a base current to one of the two transistors upsets the bridge voltage and the servo controller chip responds by running the actuator in the appropriate direction. By applying a current to the base of the other transistor, the actuator may be operated in the opposite direction as the polarity of the bridge voltage is reversed. A trimmer potentiometer installed as one of the bridge resistances allows for convenient balance adjustment.

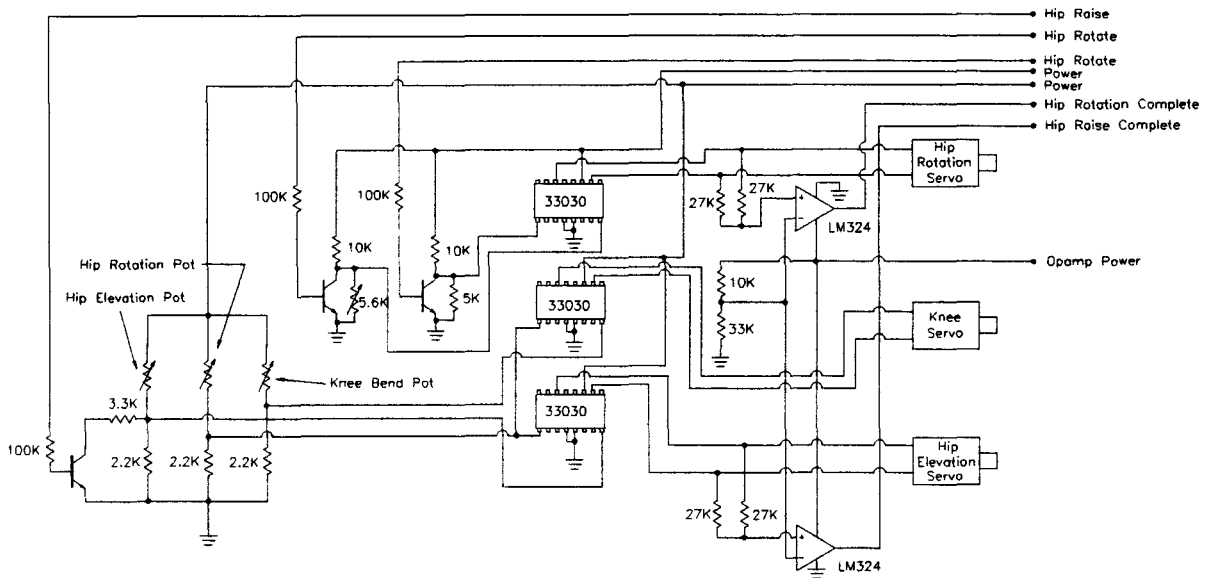


Figure 7. Servo Control Circuit

Process Feedback Signal Generation

During actuator motion, there exists a voltage differential across the motor terminals that is approximately equal to the supply voltage. Upon reaching the extremes of joint motion, whether hip rotation or elevation, the actuators cease motion automatically. In the case of hip rotation, the motion is halted through the use of limit switches; with hip elevation, motion ceases when a balance is achieved between the reference voltage inputs of the servo controller. In either situation, by virtue of the servo controller chip design, the voltage level with respect to ground at both terminals on the motor is the supply voltage (nominally 12 VDC).

This phenomenon was exploited to determine whether or not the motor is running. A voltage divider consisting of two 27kΩ resistors is connected across the motor terminals; the voltage at the junction of the resistors is sampled at the non inverting input of an LM324 operational amplifier, used as a voltage comparator. A second voltage divider consisting of a 10kΩ and a 33kΩ resistor is connected from the power supply to ground. The voltage at this junction becomes a reference voltage to which the voltage at the non inverting input is compared. The reference voltage is sampled at the inverting input of the op amp comparator.

During motion, the voltage at the non inverting input of the comparator is approximately equal to 6 VDC by the voltage divider formula,

$$\begin{aligned} V_{\text{junction}} &= V_{\text{differential}} [r1/(r1+r2)] \\ &= 12 \text{ VDC} [27\text{k}\Omega/(27\text{k}\Omega+27\text{k}\Omega)] \\ &= 6 \text{ VDC} \end{aligned}$$

The voltage at the inverting input is given by,

$$\begin{aligned} V_{\text{junction}} &= V_{\text{supply}} [r1/(r1+r2)] \\ &= 12 \text{ VDC} [33\text{k}\Omega/(33\text{k}\Omega+10\text{k}\Omega)] \\ &= 9.2 \text{ VDC} \end{aligned}$$

Since the voltage at the inverting input of the comparator is greater than that at the non inverting input, the output voltage of the comparator is 0 VDC (with a unipolar power supply for the comparator).

When motion ceases, the voltage at the junction of the motor voltage divider is equal to the supply voltage, since no current flows through the divider; this causes the voltage at the non inverting input to be 12 VDC.

Since the non inverting input voltage (12 VDC) is now greater than the voltage at the inverting input (9.2 VDC), the output of the comparator becomes approximately the comparator supply voltage (12 VDC). This and a duplicate circuit is used for process feedback from the hip rotation actuator and the hip elevation actuator. No feedback is necessary from the knee actuator as it is assumed that its position is determined by the position of the hip rotation joint and is not explicitly controlled by the microprocessor.

POWER SUPPLY

The power for the robot will be supplied by two lithium batteries (Appendix C). The batteries are Eternacell® BA-5590/U series, produced for the US military by Power Conversion, Inc. The battery consists of two-twelve volt cells which were used in parallel for a total of 12 volts (nominal). Each individual cell circuit contains a thermal switch and a 2.25 amp fuse and will supply a nominal current of 2 amps. By using 2 batteries with all cells in parallel, a total current of 8 amperes may be safely drawn.

THE CONTROL INTERFACE SYSTEM

The controller interface circuit board has several functions: power distribution, control signal routing and process feedback coordination. The board is composed of two 74HCT08 quad "AND" gates, four reed relays for power distribution, two octal SPST DIP switch packages, two 7805 5VDC voltage regulators, and supporting circuitry. The interface is organized into two main sections, each controlling the actions of, and receiving feedback signals from three legs forming a "tripod" (from the alternating tripod gait terminology). Figure 8 depicts the interface circuit.

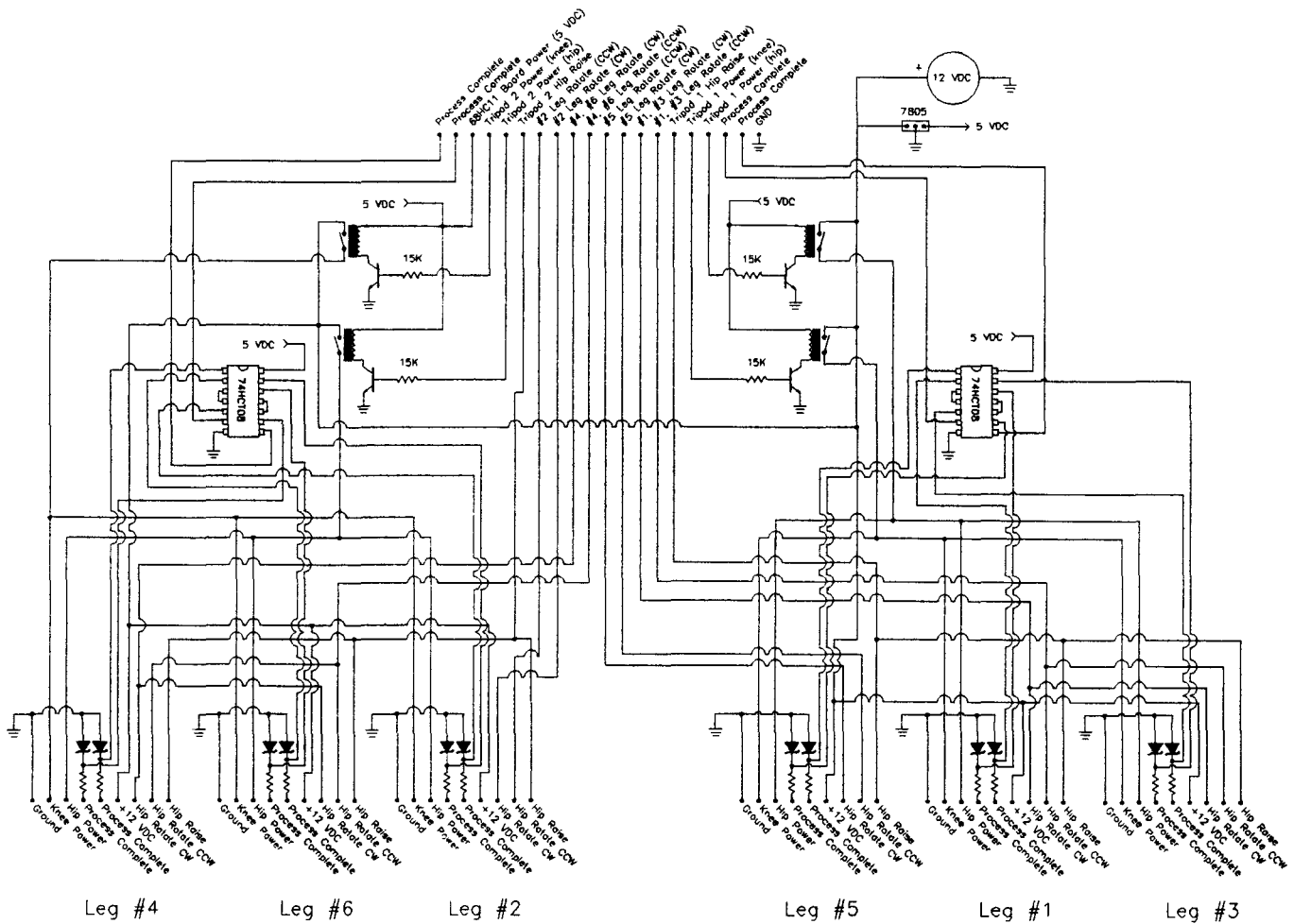


Figure 8. Interface Circuit

Tripod 1 is made up of the front and rear legs on the right side of the chassis and the middle leg of the left side; tripod 2 is made up of the front and rear legs on the left side of the robot and the middle leg on the right side. Since the legs of a tripod always operate together, the legs in each tripod share 2 common power distribution relays and a quad "AND" gate.

Interface Operation

Control signals come to the interface from one of two sources: they may be sent from the microcontroller directly, or alternately from a manual control switch box. The power/signal bus from the microcontroller consists of 20 lines: power (5VDC), ground, 4 feedback lines, and 14 motion control lines. The power/signal bus from the switch box consists of 16 lines: power, ground, and 14 motion control lines. No feedback lines were needed for manual control (switch box). The octal SPST DIP switches were installed between the microcontroller inputs and the switch box inputs to isolate the microcontroller from the switch inputs, preventing possible damage to the microcontroller during manual operation. During manual control, the switches are set to the "off" state; if microprocessor control is desired, the switches are returned to the "on" state after the switch box is unplugged from the robot.

The motion control signals pass directly to the signal output connections of the interface board, where they continue on to the servo controller boards via ribbon cables. Power distribution to the servo controller boards is controlled by the four relays. Two relays are used for each tripod; one supplies power to the three hip rotation actuators of the tripod, while the other supplies power to the six hip elevation and knee servos of the tripod. This is done so that power consumption is minimized during motions which do not require all nine actuators in the tripod to run simultaneously. The relays are controlled by bipolar junction switching transistors which are in turn controlled by the four power distribution signals from the microcontroller or switch box. All signal levels in the interface are nominally 5 VDC; voltage is controlled by the 7805 voltage regulators, one of which supplies power to the relay coils, the other supplying power to the "AND" gate ICs and microcontroller.

Process Feedback

The process feedback loop is designed to return a logic high signal back to the microcontroller after leg motion is complete. This is accomplished through the use of two 74HCT08 quad "AND" gate ICs. By design, each 74HCT08 contains four, dual input "AND" gates; by connecting the outputs of two of the gates to one of the inputs of each of the two remaining gates, the IC is configured to create two triple input "AND" gates.

Each servo controller board has two "process complete" signal lines: one signal indicates the completion of the hip raising or lowering process, the other indicates completion of the hip rotation process through the use of limit switches, whether it be clockwise or counter-clockwise rotation [2]. From the servo controller board, these signals are sent to the interface board where their voltage levels are dropped to 5VDC by reverse-biased zener diodes in series with current control resistors.

[2] See *Servo Control Circuitry* for an explanation of how the signal is generated by the servo controller board.

The "hip rotation complete" signal line is connected to an input of one of the triple input "AND" gates in the reconfigured 74HCT08; the "hip elevation complete" signal line is connected to an input of the other triple input "AND" gate on the same chip. The "process complete" signal lines from the other two legs in the tripod are similarly connected to the remaining inputs of the 74HCT08. See Figure 9 for details.

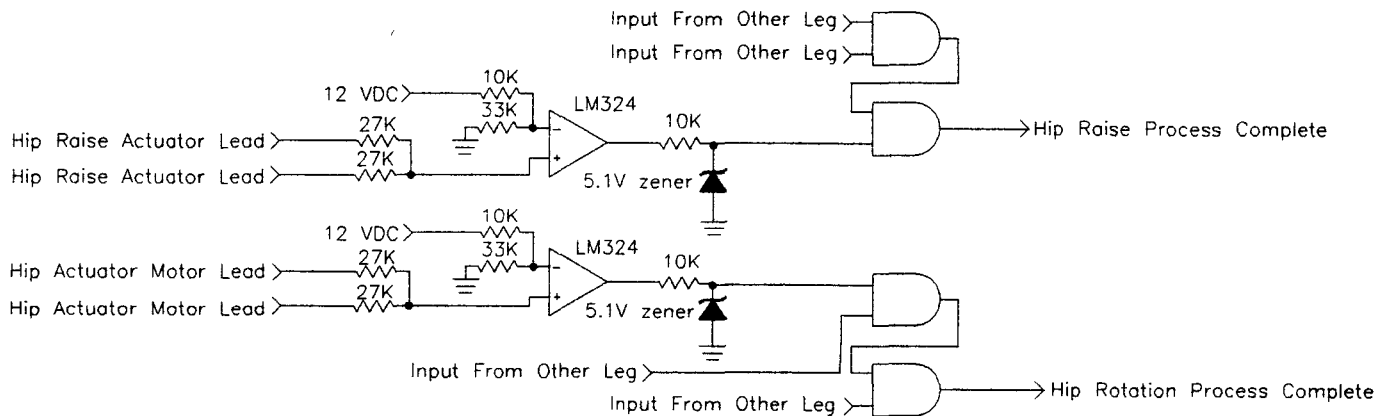


Figure 9. Process Feedback

THE MICROCONTROLLER SYSTEM

The control system consists of an MC68HC11 microcontroller and supporting circuitry. A printed circuit board with all necessary components was available off-the-shelf specifically for this microcontroller and was used as the basis for the control circuitry (Appendix F). A second printed circuit board was designed to carry other external circuitry required for obstacle sensing. A detailed report of the configuration and programming of the microcontroller is available in a separate report by Christopher Johnson in the Northern Illinois University Electrical Engineering Department.

SENSORS

There are several different types of sensing systems on board the robot. The first two types which include the hip rotation limit switches and process feedback systems (already described), are proprioceptive sensors in that they monitor the internal state of the robot. The third sensor used on board is the collision detection sensor, consisting of two antennae which project out in front of the chassis and send a digital signal directly to the microcontroller when in contact with obstacles. By using a separate antenna for the right and left side of the robot, the robot may be programmed to respond differently to obstacles depending on their location.

THE WALKING ALGORITHM

During straight walking, the robot uses an alternating tripod gait, that is, the front and rear legs on one side of the robot and the middle leg on the other side are employed during the propulsion stroke, while the remaining legs remain idle in the raised forward position. Upon completion of the propulsion stroke by the first set, the second tripod is lowered. The first tripod is then raised and moved to the forward idle position. The second tripod then propels the robot forward. Subsequently, the cycle repeats itself. In order to ensure that there is no excessive current being drawn, at no time do both sets run simultaneously.

There was no circuitry designed explicitly to approximate the leg trajectories required for minimum foot slippage during direction changes (rotation) because of the difficulty in designing an analog system to accomplish this. Therefore, it was decided that rotation would be implemented by using the same paths as for forward motion, but by rotating the legs in opposite directions. During rotation, as with forward motion, all actuators are used to turn the robot. However, rather than positioning all legs of the idle tripod in the forward position, the legs are positioned such that the front and rear legs of the idle tripod are in either the front or rear position (depending on rotation direction), while the middle leg on the opposite side is positioned in the opposite direction, i.e. if the front and rear legs on the right side of the chassis are in the forward position, the middle leg on the left side is in the rear position. The first tripod propels the rotation, while the second remains in the idle position.

Upon completion of the propulsion stroke by the first tripod, the second lowers. Tripod 1 is then raised and moved to the idle position. Tripod 2 then propels the rotation. The cycle then repeats itself until the desired rotation angle is complete. Figure 10 depicts various leg configurations for straight line motion as well as rotation.

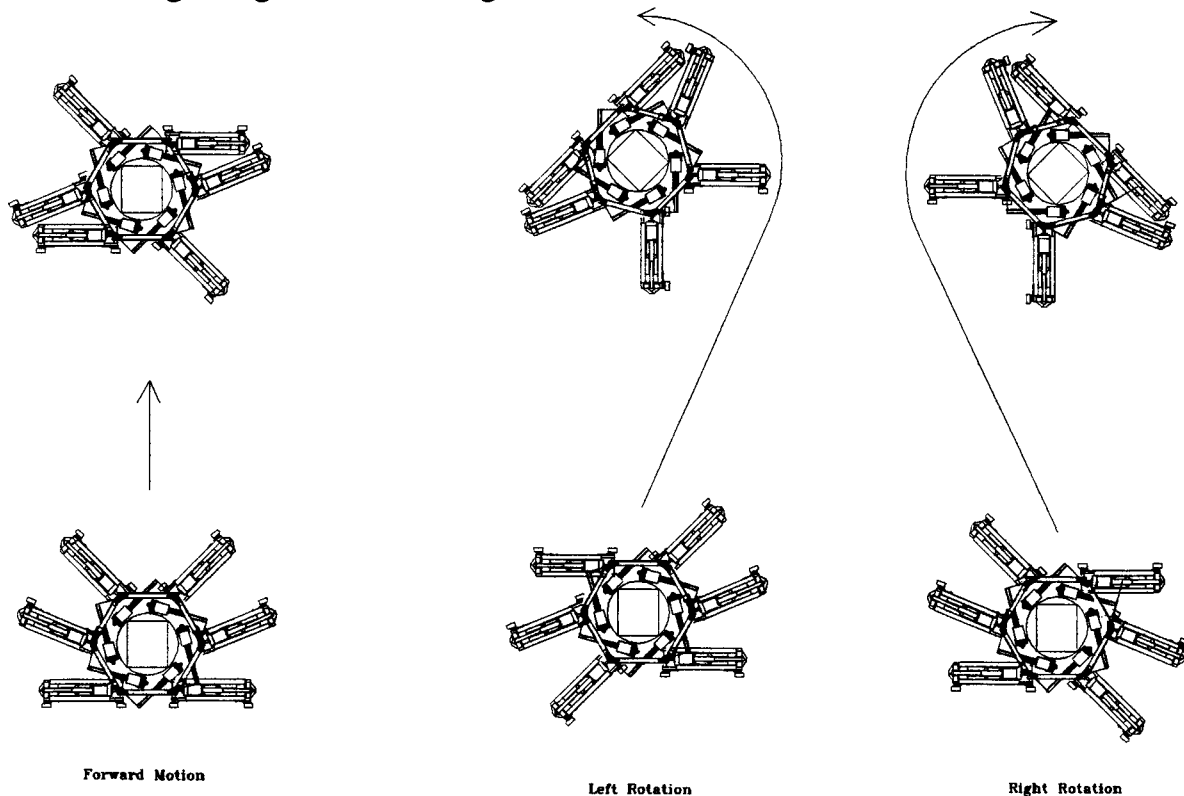


Figure 10. Leg Configurations During Motion

DESIGN PROGRAM

Table 1 depicts the development program that was followed .

Table 1. Program Development

Program Event	1995					1996				
	Aug	Sept	Oct	Nov	Dec	Jan	Feb	Mar	Apr	May
Body Design	X	X								
Body Construction		X	X	X	X					
Actuator Development	X	X	X	X	X					
Actuator Prototype	X									
Final Actuator Construction					X	X	X			
Leg Design		X	X	X	X					
Leg Construction			X	X	X	X				
Completion Of Mechanical						X				
Mechanical Debugging					X	X	X			
Servo Control Design	X	X	X	X	X	X				
Servo Interface Design					X	X	X			
Controller Design/Programming					X	X	X	X		
Electronic Construction					X	X	X	X	X	
Completion Of Electrical									X	
Electrical/Program Debugging						X	X	X	X	X

Approximate Cost Of Materials:

Motors:	\$40.50
Electronics:	
Microcontroller:	\$30.00
Microcontroller Board	\$25.00
Servo Controllers:	\$104.76
Circuit Board Kits:	\$50.00
Misc Electronic Parts:	\$100.00
Assorted Mechanical Hardware:	\$40.00
Chassis Materials:	Scrap
 Total:	 \$390.26

DISCUSSION OF RESULTS

The mechanical components of the robot functioned as designed. The actuators were capable of producing enough force to lift the weight of the chassis in all leg positions, and the range of motion of the joints was such that a wide variety of motion trajectories were possible, had the robot been endowed with the appropriate electrical systems.

The electrical systems did not perform as well as expected, however. The robot suffered from sluggish and sometimes intermittent performance. It was determined that RF interference generated by the motors cause conflicting signals in both digital and analog circuits.

While low speeds were characteristic of the design, due to the high mechanical advantage of the actuators, the actuators often appeared to be "laboring" when driven by the servo controller boards, even though no such behavior was noted when the motors were powered directly by the batteries. One conclusion is that the 33030 servo controller ICs were unable to supply enough current to the motors when demand was high. This is unlikely, however in light of the fact that the 33030 is capable of supplying 1.0 amp of current and maximum current demand under load was measured at approximately 0.600 amps. A more likely explanation of the relatively low performance of the circuitry was low signal to noise ratio, caused by the lack of signal amplification, filtering, and buffering circuitry; these conditions are easily rectified.

Future improvements to the design will incorporate these features, as well as optical isolation circuits to prevent signal noise from entering the digital electronics. Ideally, there will be a 68HC11 microcontroller for each leg, directly monitoring the three joints in the leg and reporting back to and receiving signals from a central processor. The 33030 ICs could be eliminated in such a case, with the microcontroller directly controlling power MOSFET transistors which would supply power to the actuators.

CONCLUSION

The walking robot that resulted from this design project represents the culmination of study in many fields of engineering. Due to time constraints, it lacks the refinement of its more complex counterparts; some of its design is a compromise between functionality and the realities of implementation. It has many favorable features, not the least of which is its modular construction. Its design may be easily modified, making it especially useful for research into improved walking robot design. Even without modification, enough flexibility was incorporated into its design to allow unhindered future development in control systems, behavioral programming and sensor research. Although the electrical systems require improvement, they function well enough to demonstrate successfully the operation of the mechanism.

BIBLIOGRAPHY

Shigley, J. E. and Mischke, C. R., Mechanical Engineering Design, Fifth edition, McGraw-Hill, Inc., New York, New York, 1989

Jones, J. and Flynn, A., Mobile Robots, Inspiration To Implementation, AK Peters, Wellesley, MA, 1993

Cavicchi, T. J., Fundamentals Of Electrical Engineering, Prentice Hall, Englewood Cliffs, NJ, 1993

Erdman, A. G., and Sandor, G. N., Mechanism Design-Analysis And Synthesis, Second edition, Prentice Hall, Englewood Cliffs, NJ, 1991

ACKNOWLEDGMENTS

The author would like to thank the following individuals:

Jim Hlinka, Project Engineering Manager, AO Smith Harvestore Products Inc., DeKalb, IL.

John Fidler, Department Of Electrical Engineering, Northern Illinois University, DeKalb, IL.

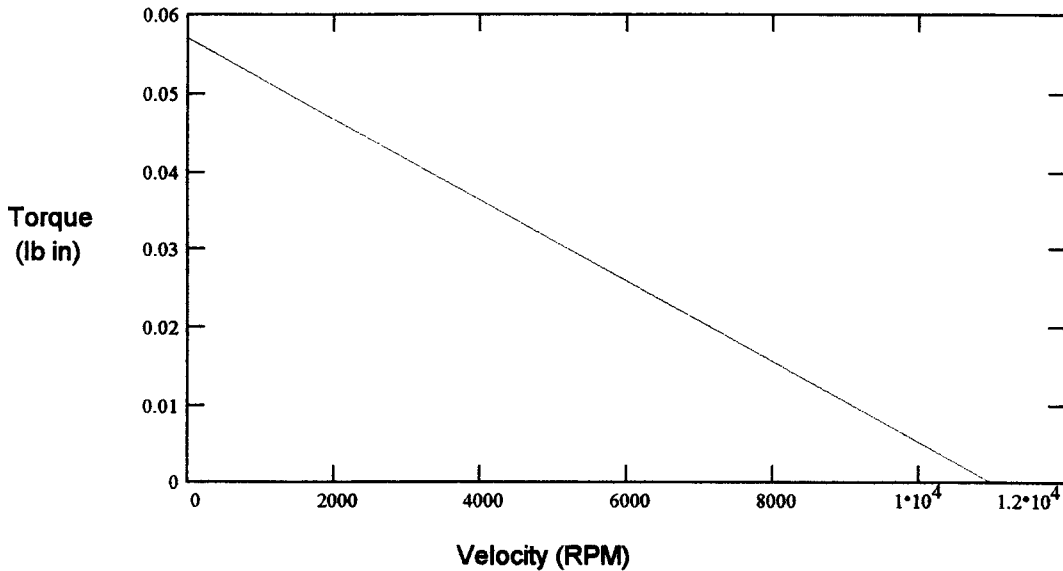
Al Metzger, College Of Engineering, Northern Illinois University, DeKalb, IL .

Dr. Peter Nagy, Ph.D, PE, Department Of Mechanical Engineering, Northern Illinois University, DeKalb, IL.

Appendix A Analysis of linear actuator design

$$v := 0..11000$$

$$\tau_v := -5.18182 \cdot 10^{-6} \cdot v + .057 \quad (1) \quad \text{The torque/velocity relationship for the motor is shown:}$$



At motor speeds approaching stall (1 RPM), the torque is at a maximum:

$$\tau_{\max} := .057$$

$$\phi := 14.5 \quad \text{Pressure angle} \quad \phi_r := \frac{\phi \cdot \pi}{180} \quad \text{Converting to radians}$$

$$d_1 := .25$$

$$d_2 := 1 \quad \text{The diameters of the gears}$$

$$d_n := .164 \quad \text{Nominal diameter of leadscrew and idler gear shaft}$$

Find the motor speed:

$$v_{\max} := 1 \quad v_{r\max} := \frac{v_{\max} \cdot 2 \cdot \pi}{60} \quad v_{r\max} = 0.105$$

$$P := v_{r\max} \cdot \tau_{\max} = 1.515 \cdot 10^{-4} \quad \text{Converting to Horsepower} \quad P = 9.043 \cdot 10^{-7}$$

Calculate the radial and tangential forces in the geartrain:

$$F_t := \frac{33000 \cdot P}{\pi \cdot d_1 \cdot \frac{v_{\max}}{12}} \quad F_t = 0.456$$

$$F_r := F_t \cdot \tan(\phi_r) \quad F_r = 0.118$$

$$F_{12t} := F_t \quad F_{12t} = 0.456 \quad \text{Tangential and Radial force components}$$

$$F_{12r} := F_r \quad F_{12r} = 0.118 \quad \text{of the pinion on the idler.}$$

Approaching stall, with a gear reduction of 16:1, the output shaft velocity is $1/16 = 0.06$ RPM

$$v_{out} := \frac{v_{max}}{16} \quad v_{out} = 0.063$$

If the power remains constant, then the torque on the leadscrew is 16 times the torque on the pinion. Therefore, the leadscrew torque w/o friction is 0.912 lb*in.

$$\tau_{ls} := 16 \tau_{max} \quad \tau_{ls} = 0.912$$

$$F_{43t} := \frac{\tau_{ls}}{\left(\frac{d_2}{2}\right)} \quad F_{43t} = 1.824$$

$$F_{43r} := F_{43t} \cdot \tan(\phi_r) \quad F_{43r} = 0.472$$

$$F_{23x} := -F_{12r} + F_{43r} \quad F_{23x} = 0.354 \quad \text{Force on the idler shaft in the x-direction}$$

$$F_{23y} := F_{12t} - F_{43t} \quad F_{23y} = -1.368 \quad \text{Force on the idler shaft in the y-direction}$$

The idler shaft reaction force is:

$$F_{idler} := \sqrt{F_{23x}^2 + F_{23y}^2} \quad F_{idler} = 1.413$$

The leadscrew reaction force is:

$$F_1 := \sqrt{F_{43r}^2 + F_{43t}^2} \quad F_1 = 1.884$$

Calculate maximum allowable load force on the actuator:

The counter torque exerted by friction between the gear shafts and gearbox must be subtracted from the maximum theoretical (no friction) leadscrew torque to get the available torque:

$$\beta_2 := .15 \quad \text{coefficient of friction}$$

$$\tau_{avail} := \tau_{ls} - \frac{\beta_2 \cdot d_n}{2} \cdot (F_{idler} + F_1) \quad \tau_{avail} = 0.871$$

At the maximum allowed motor torque, the input torque must be balanced by the thrust torque and the torque exerted by the leadscrew. If the coefficient of friction between the leadscrew drive gear and the gearbox is given above, and the motor is about to stall, the torque exerted by the sum of the thrust load torque and the screw torque is equal to the available torque.

Taking the load to be applied at the average radius of a thrust collar with a given OD and ID:

OD := .28	OD of collar	l := .031	Pitch of the drive screw
ID := .165	ID of collar	d _m := .1484	Mean diameter of the leadscrew
$R_{av} := \frac{OD + ID}{4}$	Average radius of collar	μ _s := .15	Coefficient of friction for the screw
R _{av} = 0.111		α := $\frac{30 \cdot \pi}{180}$	Thread angle

The frictional torque supplied by the load force is a function of the load force (l_{max}), the coefficient of friction at the collar (β₂), and the average radius of the collar (R_{av}). Combining this torque with the torque on the leadscrew, we then set this equal to the available torque and solve for the maximum load force that will be exerted by the ram at the highest possible motor torque output:

$$l_{max} := \frac{\tau_{avail}}{\frac{d_m}{2} \cdot \left(\frac{1 + \pi \cdot \mu_s \cdot d_m \cdot \sec(\alpha)}{\pi \cdot d_m - \mu_s \cdot l \cdot \sec(\alpha)} \right) + \beta_2 \cdot R_{av}}$$

l_{max} = 25.128 **Maximum possible load force (lbf) exerted by leadscrew with thrust and bearing friction accounted for. (at static equilibrium)**

Calculate the bearing stresses in the geartrain and leadscrew collar:

A_b := 0.041

$\sigma_{bi} := \frac{F_{idler}}{A_b}$ σ_{bi} = 34.465 **Bearing stress on the idler (PSI)**

$\sigma_{bl} := \frac{F_l}{A_b}$ σ_{bl} = 45.951 **Bearing stress on the leadscrew (PSI)**

$\sigma_{bc} := \frac{l_{max}^4}{\pi \cdot (OD - ID)^2}$ σ_{bc} = 2.419 · 10³ **Bearing stress on collar (PSI)**

Determine the idler gear shaft bore necessary for shrink fit.

$$\beta_1 := 0.8 \quad (\text{coefficient of friction for like metals, no lubrication}) \quad T_{\text{idler}} := F \cdot 12t \cdot \frac{d_2}{2} \quad T_{\text{idler}} = 0.228$$

$$F_f := \frac{T_{\text{idler}}}{\left(\frac{d_n}{2}\right)} \quad F_f = 2.78 \quad \text{Frictional force (lbf) applied on shaft.}$$

$$F_n := \frac{F_f}{\beta_1} \quad F_n = 3.475 \quad \text{Normal force (lbf) applied on shaft.}$$

$$A_{\text{shaft}} := \pi \cdot d_n \cdot l \quad \text{Circumferential area of the shaft in contact with the gear.}$$

$$P_s := \frac{F_n}{A_{\text{shaft}}} \quad P_s = 67.452 \quad \text{Minimum pressure (PSI) needed for no slippage.}$$

$$E := 30 \cdot 10^6 \quad r_i := 0 \quad r_o := .5 \quad R := \frac{d_n}{2}$$

Arbitrarily choosing a hole size that is 0.0005 in under the shaft diameter:

$$\delta := \frac{d_n}{2} - \left(\frac{d_n - .0005}{2}\right) \quad \delta = 2.5 \cdot 10^{-4}$$

$$P_t := \left[\frac{(r_o^2 - R^2) \cdot (R^2 - r_i^2)}{2 \cdot R^2 \cdot (r_o^2 - r_i^2)} \right] \cdot E \cdot \frac{\delta}{R} \quad P_t = 4.45 \cdot 10^4 \quad \text{Pressure at transition of shrink fit (PSI)}$$

So a hole in the idler gears that is .1635 in (.0005" under the size of the shaft) will be more than adequate to supply the needed pressure to transmit the torque without slippage.

Appendix B Joint Relationships

The joint angle relationships are modeled below. In a strict sense, these are not the inverse kinematic equations for motion as the equations model the joint positions only for straight line motion, not for an arbitrary location of the end effector. However, due to the limited number of trajectories used, the equations below are adequate.

Placement of a leg in the kinematic home position would result in the leg extending straight out to the side of the robot and fully extended. As this position is physically impossible for the robot to attain, and due to the fact that the inverse kinematic matrices were not used to generate the motion equations, the joint angles given here are not all measured with respect to the kinematic home position. The hip rotation and hip elevation angles are consistent with the kinematic home position, however, the knee joint angle is represented as the angle between the upper and lower legs. This relationship is more easily intuitively grasped, and simplified adjustment of the joint as well.

$$a_n := 0..45 \quad \alpha := -22.5 \quad l_1 := 10 \quad l_2 := 9.5 \quad C_e := 8.5 \quad G := 3.5 \quad S := 6$$

$$l_{1k} := 6.71 \quad l_{2k} := 2.7 \quad \lambda := 9.2 \quad F := 8$$

Ce for side = 8.5 for a 7" stride

Ce for front = 7 for a 7" stride

$$\theta_{an} := \pi \cdot \frac{a_n + \alpha}{180} \quad \text{Hip}_{an} := \theta_{an} \cdot \frac{180}{\pi} \quad \lambda_r := \frac{\lambda}{180} \cdot \pi \quad R_{an} := \sqrt{(C_e \cdot \tan(\theta_{an}))^2 + C_e^2 + G^2}$$

$$\text{Kbend}_{an} := \frac{\arccos\left[\frac{l_2^2 - (R_{an})^2 + l_1^2}{2 \cdot l_1 \cdot l_2}\right]}{\pi} \cdot 180 \quad A_{an} := \frac{\arccos\left[\frac{-l_2^2 + (R_{an})^2 + l_1^2}{2 \cdot l_1 \cdot R_{an}}\right]}{\pi} \cdot 180 \quad \phi_{an} := \frac{\arcsin\left(\frac{G}{R_{an}}\right)}{\pi} \cdot 180$$

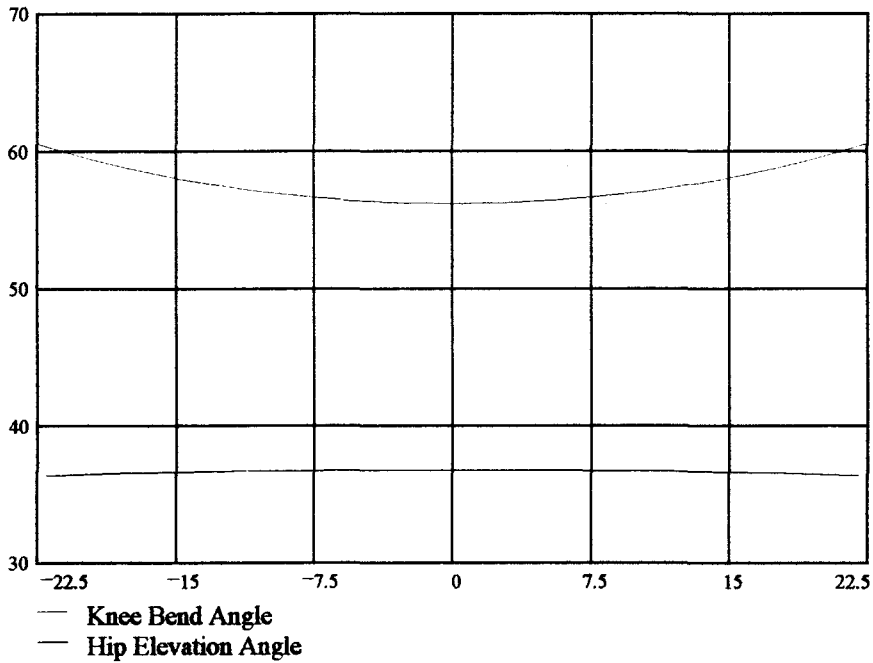
$$\text{Helev}_{an} := A_{an} - \phi_{an} \quad \text{stride} := C_e \cdot (\tan(\max(\theta)) - \tan(\min(\theta)))$$

$$\text{Helev difference} := \max(\text{Helev}) - \min(\text{Helev}) \quad \text{Kbend difference} := \max(\text{Kbend}) - \min(\text{Kbend})$$

$$F_{k_{an}} := \frac{\sqrt{l_{1k}^2 + l_{2k}^2 - 2 \cdot l_{1k} \cdot l_{2k} \cdot \cos\left(\text{Kbend}_{an} \cdot \frac{\pi}{180} - \lambda_r\right)} \cdot F \cdot l_2 \cdot \sin\left[\left(\text{Helev}_{an} + \text{Kbend}_{an} - 90\right) \cdot \frac{\pi}{180}\right]}{l_{1k} \cdot l_{2k} \cdot \sin\left(\text{Kbend}_{an} \cdot \frac{\pi}{180} - \lambda_r\right)}$$

$$F_{h_{an}} := \frac{F \cdot R_{an} \cdot \sin\left(\arcsin\left(\frac{G}{R_{an}}\right) + \frac{\pi}{2}\right)}{-l_1 \cdot S} \cdot \frac{\sin\left[\left(90 - \text{Helev}_{an}\right) \cdot \frac{\pi}{180}\right]}{\sqrt{S^2 + l_1^2 - 2 \cdot S \cdot l_1 \cdot \cos\left[\left(90 - \text{Helev}_{an}\right) \cdot \frac{\pi}{180}\right]}}$$

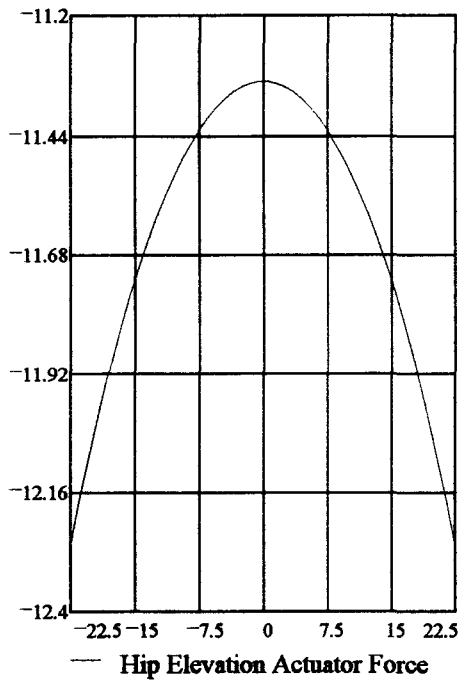
Applicable to Side Legs



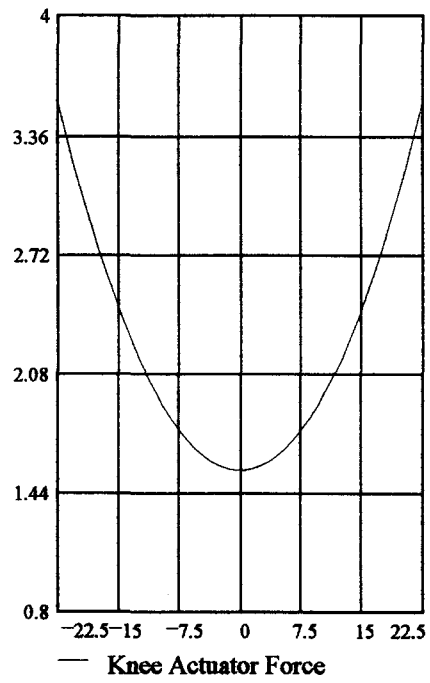
Helev difference = 0.407

Kbend difference = 4.389

stride = 7.042



Force in hip elevation actuator (lb)
vs. hip rotation angle. Negative values
indicate compression.



Force in knee actuator (lb)
vs. hip rotation angle. Negative
values indicate compression.

Dimensional Information:

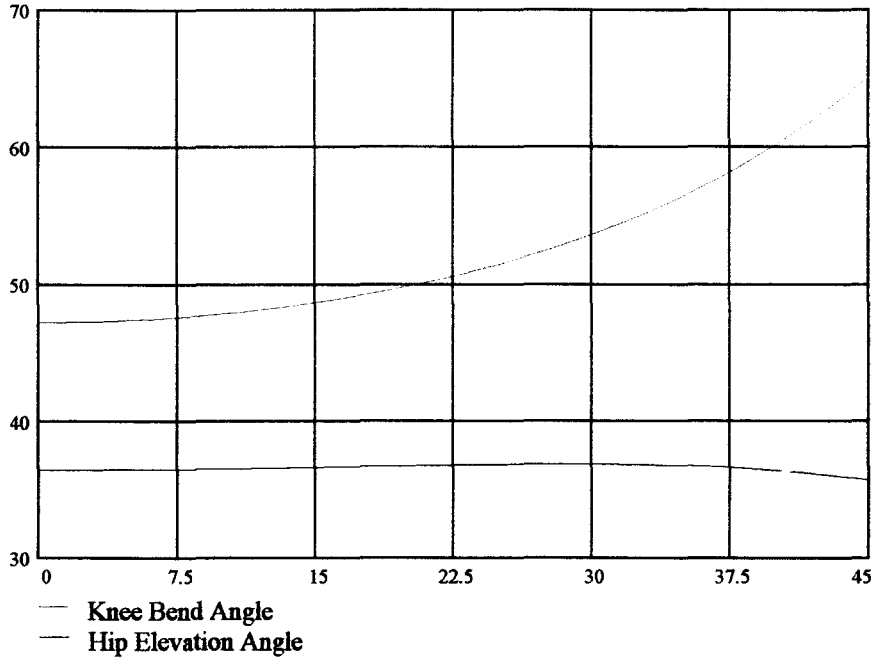
$l_1 = 10$ $l_2 = 9.5$

$S = 6$ $G = 3.5$ $\lambda = 9.2$

$l_{1k} = 6.71$ $l_{2k} = 2.7$

$F = 8$ $C_e = 8.5$

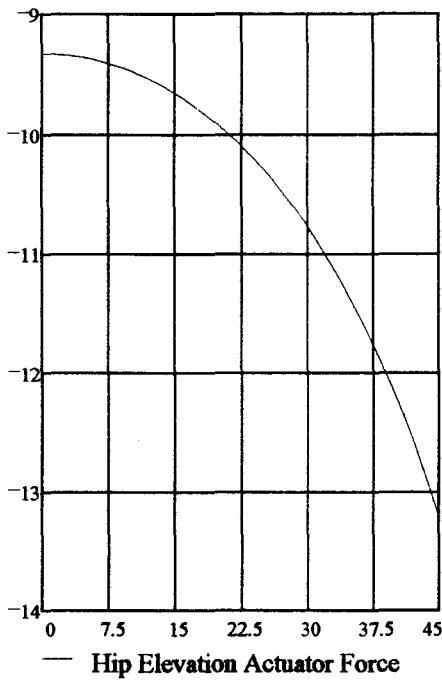
Applicable to Front and Rear Legs



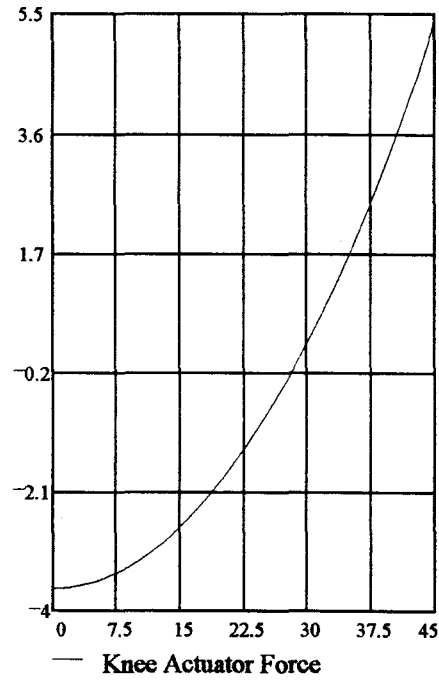
Helev difference = 1.191

Kbend difference = 17.86

stride = 7



Force in hip elevation actuator (lb)
vs. hip rotation angle. Negative values
indicate compression.



Force in knee actuator (lb)
vs. hip rotation angle. Negative
values indicate compression.

Dimensional Information:

$l_1 = 10$ $l_2 = 9.5$ $S = 6$ $G = 3.5$ $\lambda = 9.2$
 $l_{1k} = 6.71$ $l_{2k} = 2.7$ $F = 8$ $C_e = 7$

Appendix C Battery Specifications

ETERNACELL[®]

BA-5590/U

LITHIUM SULFUR DIOXIDE BATTERY, NON-RECHARGEABLE

NSN: 6135-01-036-3495

PHYSICAL SPECIFICATIONS

WEIGHT: 2.25 lbs. (max.)
 DIMENSIONS: reference space 1
 PACKAGING: plastic case

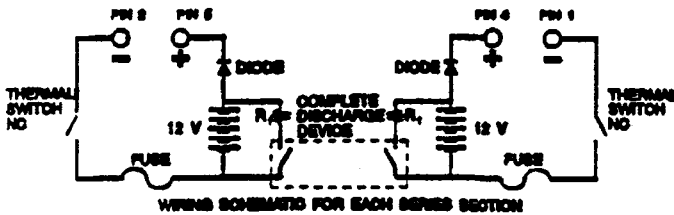
ELECTRICAL SPECIFICATIONS

BATTERY DESCRIPTION: 10 ea. STANDARD CELL SIZE 17 CELLS,
 CONSISTING OF 5 STRIPS OF 5 CELLS IN SERIES.
 2 ELECTRICAL 12 VOLT (NOM.) OUTPUTS.
 SERIES MODE (24 Volts)
 PARALLEL MODE (12 Volts)

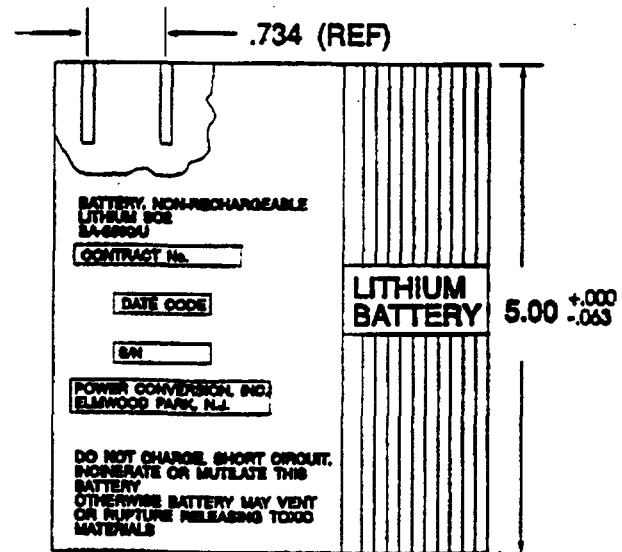
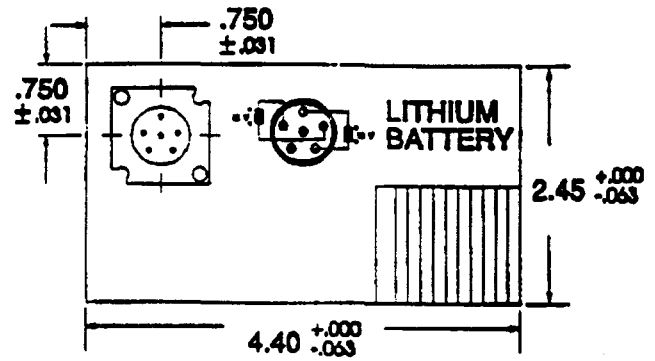
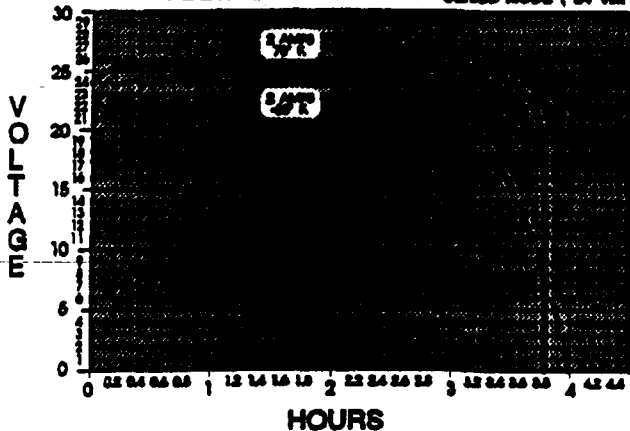
VOLTAGE	MODE:	SERIES	PARALLEL	
NOMINAL:		24 Volts	12 Volts	
OCV (max):		26.50 Volts	13.25 Volts	
USEFUL LIFE:		20 Hours	10 Hours	(END VOLTAGE)

CAPACITY	MIL-B-46480(7E)	STANDARD TEST REQUIREMENTS	AMP-HOURS
MODE:		SERIES	PARALLEL
CUT-OFF:		20 Volts	10 Volts
L TEST:		3.2 Hours	3.2 Hours
I TEST:		1.5 Hours	1.5 Hours
H TEST:		0.5 Hours	0.5 Hours

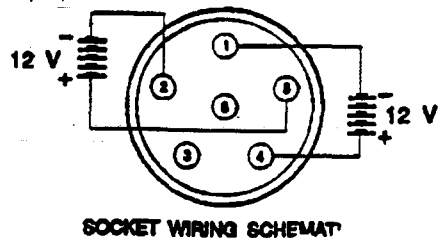
COMPONENTS:
 EACH 12 VOLT (nom.) SECTION CONTAINS:
 DIODE: TO PREVENT REVERSE CURRENT FLOW (RECHARGING)
 CURRENT FUSE: NON-REPLACABLE 3.25 AMP SLO-BLO FUSE
 THERMAL FUSE: NON-REPLACABLE NORMALLY CLOSED NON-RESETTABLE
 OPERATES AT 81°C. (186°F.)
 COMPLETE DISCHARGE DEVICE: USED TO DISCHARGE THE BATTERY TO 0 Volts AFTER
 EQUIPMENT USAGE (FOR DISPOSAL PURPOSES)
 MATING CONNECTOR: ITT CANNON CA 110621-4
 MILITARY SPECIFICATION: MIL-B-46480(7E)



MAXIMUM CONTINUOUS DISCHARGE CHARACTERISTICS VOLTAGE VS. TIME SERIES MODE (24 Volt)



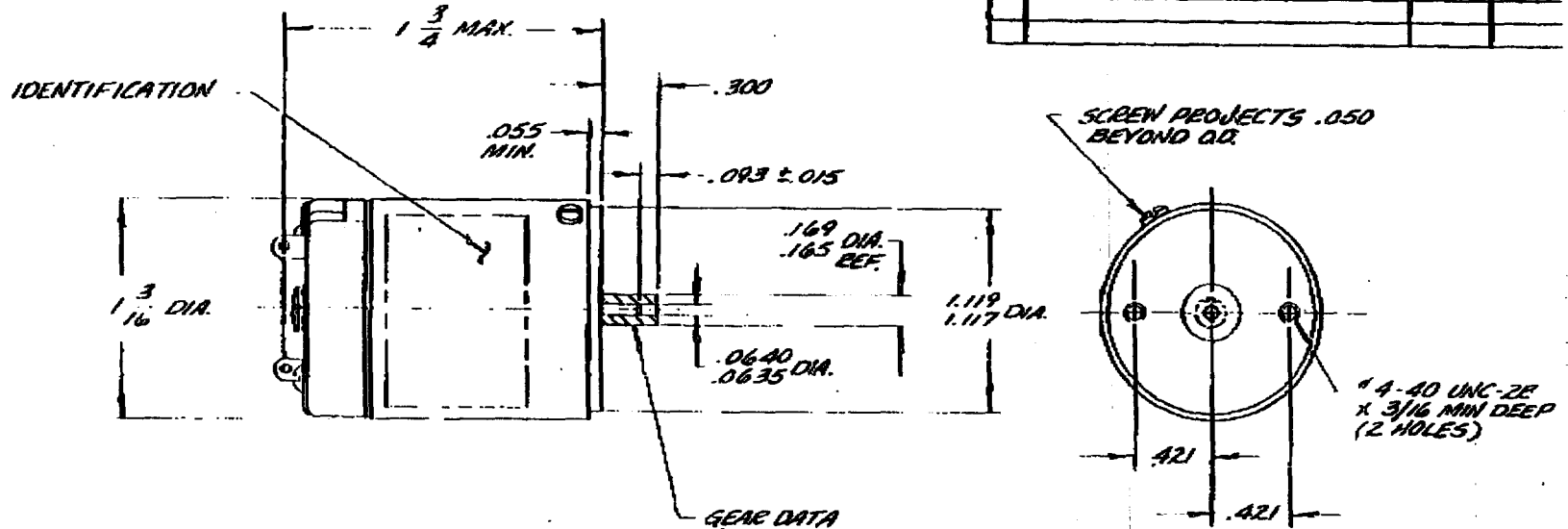
OUTLINE DIMENSIONS ARE IN INCHES



Power Conversion
 200 MIDLAND AVENUE
 SADDLE BROOK, NJ 07663
 PHONE: 201-796-4800
 800-453-1911
 FAX: 201-796-6243

Appendix D Motor Specifications
(On following page)

REVISIONS		3A683	
LTR	DESCRIPTION	DATE	APPROVE
2	REV FREDNN E20 42689	CEW 1-18-74	RS



NOTES:

- A. PERFORMANCE SPECIFICATIONS:**
- VOLTAGE RANGE: 24 TO 29 VDC. TEST VOLTAGE: 26 VDC.
 - NORMAL RATED LOAD (NRL): 1.0 IN.OZ.
 - SPEED: 24,000 RPM MAX. AT NO LOAD.
16,000 RPM MIN. AT NRL.
 - MAX CURRENT: 1.0 AMP AT NRL.
 - STALL TORQUE: 2.0 IN.OZ. MIN.
 - DUTY CYCLE: 2 SEC ON; 10 SEC OFF.
 - WHEN (+) TERMINAL IS POSITIVE & (-) TERMINAL IS NEGATIVE, ROTATION IS CLOCKWISE VIEWING SHAFT END.
 - WEIGHT: 5.0 OZ. MAX.
 - MOTOR DESIGNED TO MEET THE REQUIREMENTS OF MIL-M-8609.
- B. MECHANICAL**
- WITH SHAFT HELD STATIONARY & MOTOR ROTATED ON ITS BEARINGS RUNOUT OF 1.119/1.117 DIA. NOT TO EXCEED .004 TIR.

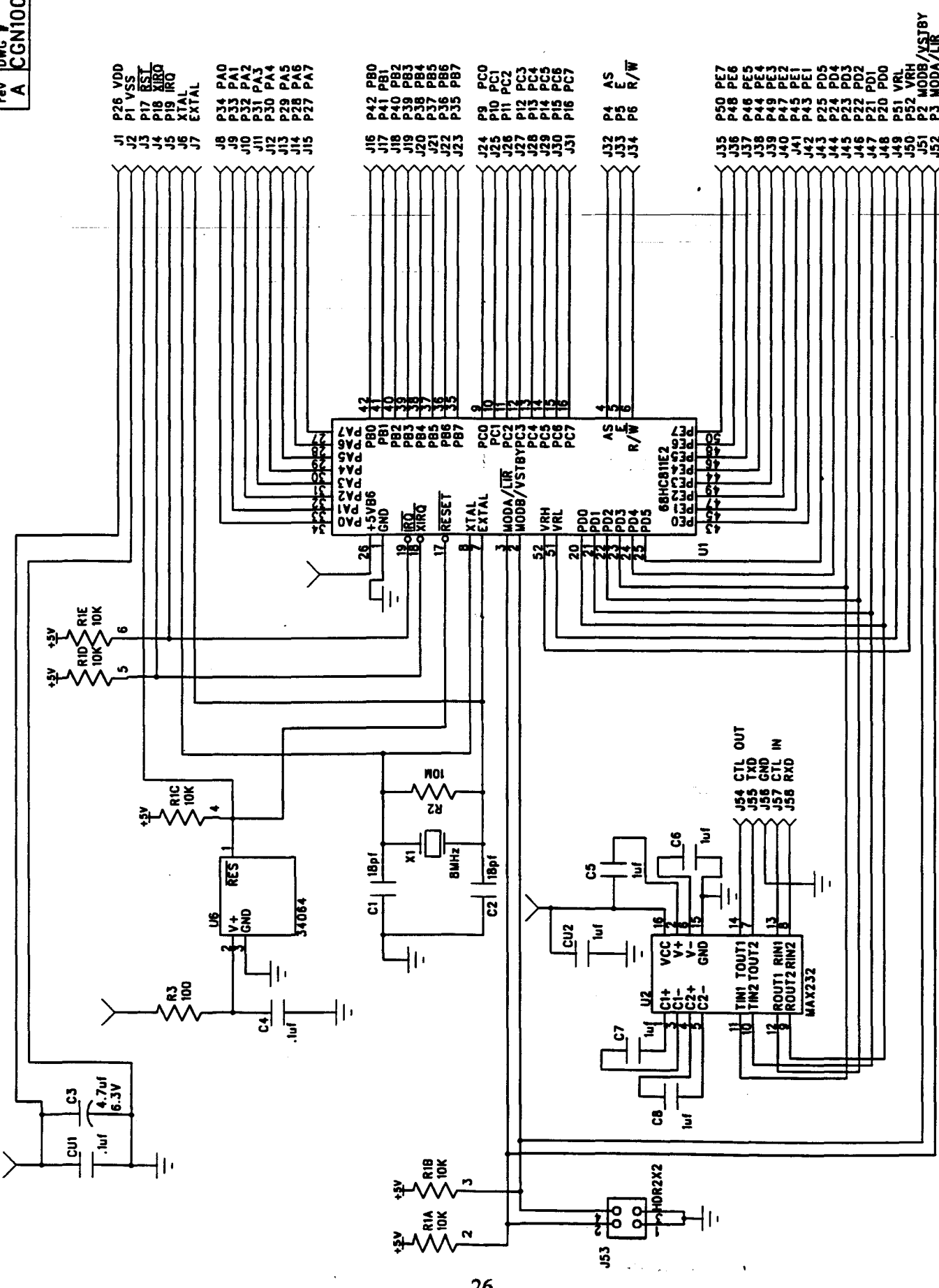
REDUCED PRINT
ISSUED
C/A JAN 29 1990

ITEM	PREFIX	LTR	BODY	SUFFIX	QUANTITY REQUIRED	DESCRIPTION	CODE IDENT
PARTS LIST							

UNLESS OTHERWISE SPECIFIED DIMENSIONS ARE IN INCHES. TOLERANCES UNLESS OTHERWISE SPECIFIED: FRACTIONS DECIMALS ANGLES ± 1/64 ± .005 ± 1°		REQ. 2160	BOOK	TWIN GLOBE MOTORS AN OPERATION OF TWIN ELECTRONIC COMPONENTS DAYTON, OHIO			
MATERIAL		DRAFTSMAN	GUTHRIE				
HEAT TREAT		CHK	GEO	DATE	TITLE MOTOR, DC - MM, OPEN, 3A-90 ARM		
COATING		ENGR	JOHNSON				
NEXT ASSY	USED ON	APPD	GEO	APPD	SIZE	CODE IDENT	ROLLING NO.
APPLICATION		APPD			C	25140	3A683
				SCALE	2:1	SHEET 1 OF 1	

DO NOT SCALE DRAWING.
TWIN GLOBE MOTORS SHOP STANDARD 635100 SUPPLEMENTS THIS DRAWING.
SPECIFICATIONS REFERENCED ON THIS DRAWING SHALL BE OF LATEST ISSUE.
THIS DRAWING IS THE SOLE PROPERTY OF TWIN INC. AND IS MADE AVAILABLE TO CUSTOMERS AND DISTRIBUTORS FOR LIMITED USE. THE INFORMATION CONTAINED ON THIS DRAWING IS CONSIDERED CONFIDENTIAL AND THE DRAWING MUST BE RETURNED AFTER IT HAS SERVED ITS PURPOSE. REPRODUCTION OR DISCLOSURE OF THIS DRAWING IS AUTHORIZED FOR ANY PURPOSES BEYOND THAT SPECIFICALLY TRANSMITTED. ANY UNAUTHORIZED USE OF THIS DRAWING SHALL BE SUBJECT TO THE PENALTIES PROVIDED UNDER LAW.

Appendix E Microcontroller Board



DESCRIPTION:

Appendix F Printed Circuit Board Layouts

Printed circuit boards were etched using a photo etch process. The circuit board kit was obtained from Kepro Circuit Systems, Inc., 630 Axminister Drive, Fenton, Missouri, 63026-2992, Tel 1-800-325-3878. Kit is catalog # DFP-101B.

Three types of circuit boards were designed for the robot: a servo controller board, an interface board, and a processor board. The board designs are shown on page 28 in full scale from top to bottom in the order listed .

The etching process required that a negative image of the circuit be made on a clear overlay. Photo reversing film was available from the manufacturer, however it was more expedient to create the circuit with CAD software, print it on paper with a laser printer, and have the negative image made on a transparency using a color copier. This process not only saved time and money, it made it far easier to correct mistakes in a timely fashion.

The etching process was as follows: The circuit overlay was placed over the photo-sensitive circuit board which was then exposed to direct sunlight for approximately 18-20 seconds. The circuit board was allowed to cure for 15 minutes in darkness prior to developing. Upon curing, the board was developed in the solution supplied with the kit and etched in the normal manner using ferric chloride etchant. After etching and drilling, the components were soldered onto the boards and tested for proper function.

